TU Delft

Delft University of Technology

Performance comparison of analytical models for rotor eccentricity
A case study of active magnetic bearing

Cao, Zhi; Huang, Yunkai; Guo, Baocheng; Dong, Jianning; Peng, Fei

DOI
10.4283/JMAG.2020.25.2.285

Publication date
2020

Document Version
Accepted author manuscript

Published in
Journal of Magnetics

Citation (APA)
Cao, Z., Huang, Y., Guo, B., Dong, J., & Peng, F. (2020). Performance comparison of analytical models for rotor eccentricity: A case study of active magnetic bearing. *Journal of Magnetics*, *25*(2), 285-292. https://doi.org/10.4283/JMAG.2020.25.2.285

Important note
To cite this publication, please use the final published version (if applicable).
Please check the document version above.

Copyright
Other than for strictly personal use, it is not permitted to download, forward or distribute the text or part of it, without the consent of the author(s) and/or copyright holder(s), unless the work is under an open content license such as Creative Commons.

Takedown policy
Please contact us and provide details if you believe this document breaches copyrights.
We will remove access to the work immediately and investigate your claim.

This work is downloaded from Delft University of Technology.
For technical reasons the number of authors shown on this cover page is limited to a maximum of 10.

Performance Comparison of Analytical Models for Rotor Eccentricity: A Case Study of Active Magnetic Bearing

Zhi Cao [1], Yunkai Huang [1*], Baocheng Guo [2], Jianning Dong [3] and Fei Peng [1]

[1] *Southeast University, School of Electrical Engineering, Nanjing, Jiangsu, China*
[2] *State Key Laboratory of Reliability and Intelligence of Electrical Equipment, Hebei University of Technology, Tianjin, China*
[3] *Delft University of Technology, Department of Electrical Sustainable Energy, Delft, the Netherlands*

This paper applies two different analytical methods, i.e., the perturbation method and superposition method, to calculate the magnetic flux density distribution and the magnetic force of the active magnetic bearing (AMB) with the rotor eccentricity. These two methods are thoroughly analyzed, compared and validated by the finite element model (FEM). The perturbation method is theoretically complex while the superposition method is intuitive. The valid range of the superposition method is larger than the perturbation method. However, the superposition method requires longer computation time. The main contribution of this paper is assessing the effectiveness of two analytical methods for predicting the AMB performance with the rotor eccentricity and giving a comprehensive guideline for engineers to choose the proper analytical method to design AMB.

Keywords: Active magnetic bearing (AMB), analytical models, sub-domain method, perturbation method, superposition method

*Corresponding author: Tel:+86-15651627932, Fax: +86-83791696
e-mail: huangyk@seu.edu.cn

1. Introduction

Active magnetic bearing (AMB), compared with conventional mechanical bearings, is promising in many critical high-speed industrial applications such as flywheel systems, turbo-machinery, and vacuum systems due to its outstanding features, i.e., contactless operation, no lubrication needed, no mechanical wear and ability to actively control rotor dynamics [1]. The rotor of the AMB system usually operates at the eccentric state, and it is necessary to analyze the performance including the magnetic density flux distribution and magnetic force under rotor eccentricity conditions to facilitate the design and control.

Comparing with the finite element model (FEM), the analytical models (AMs), such as the sub-domain method, require lower CPU resources while having acceptable accuracy. Therefore, they are widely adopted by engineers. As for the AMB, the rotor is always under the eccentricity condition when the load or speed changes. Hence, performance evaluation is an important issue for designers. AMs are regarded as an effective approach to deal with the eccentricity calculation since significant eccentricity conditions should always be accounted for. Two AMs are widely used to solve the eccentricity problems. The first one is the perturbation method [2]–[4], which only considers up to the first-order term by Taylor series expansion within a small eccentricity range, and the other one deploys the superposition method [5], [6] in which the original eccentric state is first divided into several concentric states to consider then to be superposed.

However, the previous work only focuses on the respective analysis and application of two methods. The difference in the performance like effectiveness range and efficiency of two methods has never been researched. Besides, these methods are mainly applied

in electrical machine analysis [7], [8]. Hence, these two methods applied in AMB analysis are thoroughly assessed and compared in this paper, which provides a guideline for designing AMB as well as electrical machines with the analytical methods considering rotor eccentricity.

This paper is organized as follows: The analytical sub-domain model of a heteropolar AMB is firstly established under the condition of rotor concentricity in section 2. Then section 3 presents two different methods to take rotor eccentricity into account. The results are presented and discussed in section 4. Finally, conclusions are drawn at the end of the paper.

2. Description of the analytical sub-domain model without eccentricity

The analytical solution is always based on the following assumptions [8]: (1) the end effect is ignored, and the vector potential **A** and current density **J** have only z-axis components; (2) the magnetic flux density vector is independent of z; (3) the stator and rotor cores are infinitely permeable so that saturation is neglected as well; (4) the axis of the rotor and stator are assumed parallel; (5) the edges of the slots are along the radius.

Fig. 1 HERE.

The simplified structure of radial heteropolar AMB is shown in Fig.1, which is divided into two sub-regions: air-gap (region I) and slots (region II). The primary geometry parameters in Fig. 1 are: R_s is the stator teeth radius; R_{sl}, the slot bottom radius; R_r, the rotor yoke radius; δ is the slot span angle; g_0 is the air-gap length. The governing partial differential equations for slots and air-gap without the eccentricity are expressed as:

$$\frac{\partial^2 A_{\mathrm{I}}^0}{\partial r^2}+\frac{1}{r}\frac{\partial A_{\mathrm{I}}^0}{\partial r}+\frac{1}{r^2}\frac{\partial^2 A_{\mathrm{I}}^0}{\partial \theta^2}=0 \qquad (1)$$

$$\frac{\partial^2 A_{\mathrm{IIj}}^0}{\partial r^2}+\frac{1}{r}\frac{\partial A_{\mathrm{IIj}}^0}{\partial r}+\frac{1}{r^2}\frac{\partial^2 A_{\mathrm{IIj}}^0}{\partial \theta^2}=-\mu_0 J_j \qquad (2)$$

where A_{I}^0 is the axial component of the zeroth-order vector magnetic potential in the air-gap. $A_{\mathrm{II}j}^0$ is the axial component of the zeroth-order vector magnetic potential in the *j*th slot. Here the zeroth-order quantities are those without rotor eccentricity.

The current density J_j in the *j*th slot shown in Fig. 1 can be expressed by[8]:

$$J_j = J_{j0}+\sum_{v=1}^{V} J_{jv}\cos\left(\frac{\pi v}{\delta}\left(\theta-\theta_j+\frac{\delta}{2}\right)\right) \qquad (3)$$

$$J_{j0}=\frac{J_{j1}+J_{j2}}{2} \qquad (4)$$

$$J_{jv}=\frac{2}{v\pi}\left(J_{j1}+(-1)^v J_{j2}\right)\sin\left(\frac{v\pi}{2}\right) \qquad (5)$$

where θ_j is the angle of the *j*th slot center. V is the maximum number of harmonics in slots. J_{j1} and J_{j2} are respectively the current density of two windings in the same slot.

By the variable separation method, the general solutions of (1)-(2) can be obtained as:

$$A_{\mathrm{I}}^0(r,\theta)=\sum_{n=1}^{N}\left[a_{\mathrm{I}n}^0\left(\frac{r}{R_s}\right)^n+b_{\mathrm{I}n}^0\left(\frac{r}{R_r}\right)^{-n}\right]\cos(n\theta)+\sum_{n=1}^{N}\left[c_{\mathrm{I}n}^0\left(\frac{r}{R_s}\right)^n+d_{\mathrm{I}n}^0\left(\frac{r}{R_r}\right)^{-n}\right]\sin(n\theta) \qquad (6)$$

$$\begin{aligned}A_{\mathrm{II}j}^0(r,\theta)=&A_{\mathrm{II}j0}+\frac{\mu_0 J_{j0}}{2}\left(R_{sl}^2\ln r-\frac{r^2}{2}\right)\\&+\sum_{v=1}^{V}\left\{a_{\mathrm{II}j,v}^0\left[\left(\frac{R_s}{R_{sl}}\right)^{E_v}\left(\frac{r}{R_{sl}}\right)^{E_v}+\left(\frac{r}{R_s}\right)^{-E_v}\right]+\frac{\mu_0 J_{jv}}{E_v^2-4}\left(r^2-\frac{2{R_{sl}}^2}{E_v}\left(\frac{r}{R_{sl}}\right)^{E_v}\right)\right\}\\&\times\cos\left[E_v\left(\theta-\theta_j+\frac{\delta}{2}\right)\right]\end{aligned} \qquad (7)$$

where $a_{\mathrm{I}n}^0$, $b_{\mathrm{I}n}^0$, $c_{\mathrm{I}n}^0$, $d_{\mathrm{I}n}^0$, $a_{\mathrm{II}j,v}^0$ are the coefficients of the zeroth-order solutions. N is the maximum number of harmonics considered in the air-gap, and

$$E_v=\pi v/\delta \qquad (8)$$

The radial and tangential components of flux density can be obtained from the vector potential distribution by:

$$B_r = \frac{1}{r}\frac{\partial A}{\partial \theta} \qquad (9)$$

$$B_\theta = -\frac{\partial A}{\partial r} \qquad (10)$$

The boundary conditions in the case of the zeroth-order equations are listed as follows:

$$H_{\mathrm{I},\theta}^{0}\left(r,\theta\right)\Big|_{r=R_r} = 0 \qquad (11)$$

$$B_{\mathrm{I},r}^{0}\left(r,\theta\right)\Big|_{r=R_s} = B_{\mathrm{IIj},r}^{0}\left(r,\theta\right)\Big|_{r=R_s}, \theta_j - \frac{\delta}{2} \le \theta \le \theta_j + \frac{\delta}{2} \qquad (12)$$

$$H_{\mathrm{I},\theta}^{0}\left(r,\theta\right)\Big|_{r=R_s} = \begin{cases} \sum_{j=1}^{Q} H_{\mathrm{IIj},\theta}^{0}\left(r,\theta\right)\Big|_{r=R_s}, \theta_j - \frac{\delta}{2} \le \theta \le \theta_j + \frac{\delta}{2} \\ 0, \text{otherwise} \end{cases} \qquad (13)$$

where H denotes magnetic field intensity, Q is the number of slots.

3. Description of two analytical methods to consider rotor eccentricity

Fig. 2 HERE.

Fig. 2 shows the rotor eccentricity and two different coordinates that are attached to the stator and rotor, respectively. The coordinate transformations of these two reference frames can be derived as follows [2]:

$$r = \rho + \varepsilon\cos(\psi - \varphi) \qquad (14)$$

$$\theta = \psi + \frac{\varepsilon}{r}\sin(\psi - \varphi) \qquad (15)$$

Here, we define the eccentricity factor as follows:

$$k_e = \varepsilon / g_0 \qquad (16)$$

A. The perturbation method

According to the perturbation approach, all the quantities are represented by the zeroth-order and first-order equations assuming a small eccentricity.

$$X(r,\theta,\varepsilon) = X^0(r,\theta) + \varepsilon X^1(r,\theta) \qquad (17)$$

where X represents quantities such as magnetic vector potential, magnetic flux density and so on, X^0 and X^1 are the zeroth-order and first-order components.

As the zeroth-order governing partial differential equations without the eccentricity have been shown in (1)-(2), the first-order governing partial differential equations are expressed as:

$$\frac{\partial^2 A_{\mathrm{I}}^1}{\partial r^2} + \frac{1}{r}\frac{\partial A_{\mathrm{I}}^1}{\partial r} + \frac{1}{r^2}\frac{\partial^2 A_{\mathrm{I}}^1}{\partial \theta^2} = 0 \qquad (18)$$

$$\frac{\partial^2 A_{\mathrm{II}j}^1}{\partial r^2} + \frac{1}{r}\frac{\partial A_{\mathrm{II}j}^1}{\partial r} + \frac{1}{r^2}\frac{\partial^2 A_{\mathrm{II}j}^1}{\partial \theta^2} = 0 \qquad (19)$$

where A_{I}^1 is the axial component of the first-order vector magnetic potential in the air-gap. $A_{\mathrm{II}j}^1$ is the axial component of the first-order vector magnetic potential in the jth slot.

The general solutions of (18) and (19) can be deducted as follows with the same method.

$$\begin{aligned} A_{\mathrm{I}}^1(r,\theta) = & \sum_{n=1}^{N}\left[a_{\mathrm{I}n}^1\left(\frac{r}{R_s}\right)^{n+1} + b_{\mathrm{I}n}^1\left(\frac{r}{R_r}\right)^{-n-1}\right]\cos\left((n+1)\theta\right) \\ & + \sum_{n=1}^{N}\left[c_{\mathrm{I}n}^1\left(\frac{r}{R_s}\right)^{n+1} + d_{\mathrm{I}n}^1\left(\frac{r}{R_r}\right)^{-n-1}\right]\sin\left((n+1)\theta\right) \\ & + \sum_{n=1}^{N}\left[e_{\mathrm{I}n}^1\left(\frac{r}{R_s}\right)^{n-1} + f_{\mathrm{I}n}^1\left(\frac{r}{R_r}\right)^{-n+1}\right]\cos\left((n-1)\theta\right) \\ & + \sum_{n=1}^{N}\left[g_{\mathrm{I}n}^1\left(\frac{r}{R_s}\right)^{n-1} + h_{\mathrm{I}n}^1\left(\frac{r}{R_r}\right)^{-n+1}\right]\sin\left((n-1)\theta\right) \end{aligned} \qquad (20)$$

$$A_{\mathrm{II}j}^{1}\left(r,\theta\right)=\sum_{v=1}^{V}\left\{a_{\mathrm{II}j,v}^{1}\left(\frac{r}{R_{sl}}\right)^{E_v}+b_{\mathrm{II}j,v}^{1}\left(\frac{r}{R_s}\right)^{-E_v}\right\}\times\cos\left[E_v\left(\theta-\theta_j+\frac{\delta}{2}\right)\right]\qquad(21)$$

where $a_{\mathrm{I}n}^{1}$, $b_{\mathrm{I}n}^{1}$, $c_{\mathrm{I}n}^{1}$, $d_{\mathrm{I}n}^{1}$, $e_{\mathrm{I}n}^{1}$, $f_{\mathrm{I}n}^{1}$, $g_{\mathrm{I}n}^{1}$, $h_{\mathrm{I}n}^{1}$, $a_{\mathrm{II}j,v}^{1}$, $b_{\mathrm{II}j,v}^{1}$ are the coefficients of the first-order solutions.

Since eccentricity occurs in the first-order problem, the boundary condition at the interface between the rotor yoke and air-gap is changed. Using the Taylor expansion and perturbation method, the boundary condition at the interface between the rotor yoke and air-gap can be obtained as [2]:

$$\left.\frac{\partial A_{\mathrm{I}}^{1}\left(r,\theta\right)}{\partial r}\right|_{r=R_r}=-\left.\frac{\partial^2 A_{\mathrm{I}}^{0}\left(r,\theta\right)}{\partial r^2}\cos\left(\theta-\varphi\right)\right|_{r=R_r}-\frac{1}{{R_r}^2}\left.\frac{\partial A_{\mathrm{I}}^{0}\left(r,\theta\right)}{\partial\theta}\sin\left(\theta-\varphi\right)\right|_{r=R_r}\qquad(22)$$

The rest of the boundary conditions are listed as follows, which is similar to the zeroth-order problem.

$$H_{\mathrm{II}j,\theta}^{1}\left(r,\theta\right)\Big|_{r=R_{sl}}=0,\theta_j-\frac{\delta}{2}\le\theta\le\theta_j+\frac{\delta}{2}\qquad(23)$$

$$B_{\mathrm{I},r}^{1}\left(r,\theta\right)\Big|_{r=R_s}=B_{\mathrm{II}j,r}^{1}\left(r,\theta\right)\Big|_{r=R_s},\theta_j-\frac{\delta}{2}\le\theta\le\theta_j+\frac{\delta}{2}\qquad(24)$$

$$H_{\mathrm{I},\theta}^{1}\left(r,\theta\right)\Big|_{r=R_s}=\begin{cases}\sum_{j=1}^{Q}H_{\mathrm{II}j,\theta}^{1}\left(r,\theta\right)\Big|_{r=R_s},\theta_j-\frac{\delta}{2}\le\theta\le\theta_j+\frac{\delta}{2}\\0,\text{otherwise}\end{cases}\qquad(25)$$

Likewise, the magnetic flux density of the first order can be obtained by taking the curl of the vector magnetic potential. And the total magnetic flux density under eccentricity can be calculated using (17). Afterward, the magnetic traction forces are computed according to Maxwell's stress tensor as follows:

$$F_x=L\int_0^{2\pi}\left[\frac{1}{2\mu_0}\left(B_{\mathrm{I},r}^{2}-B_{\mathrm{I},\theta}^{2}\right)\cos\theta-\frac{1}{\mu_0}B_{\mathrm{I},r}B_{\mathrm{I},\theta}\sin\theta\right]r_g\,d\theta\qquad(26)$$

$$F_y = L\int_0^{2\pi}\left[\frac{1}{2\mu_0}\left(B_{\mathrm{I},r}^2 - B_{\mathrm{I},\theta}^2\right)\sin\theta + \frac{1}{\mu_0}B_{\mathrm{I},r}B_{\mathrm{I},\theta}\cos\theta\right]r_g d\theta \qquad (27)$$

where L is the axial length of the AMB, r_g is the integral radius for magnetic forces, which is chosen at the center of the air-gap, and $B_{\mathrm{I},r}$ and $B_{\mathrm{I},\theta}$ are obtained radial and tangential components of the flux density at the center of the air-gap.

B. The superposition method

Fig. 3 HERE.

As is shown in Fig. 3, with the superposition method, the geometric center of the rotor is taken as the reference center, and the original eccentric AMB rotor is first divided into N_s uniform sections along the air-gap circumferential direction. According to (14), the equivalent rotor radius of each section is determined by its center as [5]:

$$R_{ri} = R_r + \varepsilon\cos\left[\frac{2\pi}{N_s}\left(i-\frac{1}{2}\right)-\varphi\right] \qquad (28)$$

Then, the equivalent rotor radius of each section is used to build up a concentric model, and the air-gap flux density of each section can be represented by the corresponding concentric model, which can easily be accounted for by the sub-domain method mentioned above. By superposition, the air-gap flux density of the original eccentric AMB can be synthesized from that of all sections as follows:

$$B_r = B_{ri}, \theta \in \left(\theta_{si}, \theta_{ei}\right) \qquad (29)$$

$$B_t = B_{ti}, \theta \in \left(\theta_{si}, \theta_{ei}\right) \qquad (30)$$

where B_r and B_t are the radial and tangential air-gap flux densities of the original eccentric model, respectively; B_{ri} and B_{ti} are the radial and circumferential air-gap flux densities of the ith concentric model; θ_{si} and θ_{ei} are the start and end mechanical angular

position of *i*th section, respectively.

Consequently, the magnetic force can be predicted by the integral of Maxwell stress tensor based on the synthesized air-gap flux density, and thus the equations (26)-(27) need to be discretized into the following form:

$$F_x = L\sum_{i=1}^{N_s}\int_{\theta_{sri}}^{\theta_{eri}}\left[\frac{1}{2\mu_0}\left(B_{\mathrm{l},ri}^2 - B_{\mathrm{l},\theta i}^2\right)\cos\theta - \frac{1}{\mu_0}B_{\mathrm{l},ri}B_{\mathrm{l},\theta i}\sin\theta\right]r_g d\theta \quad (31)$$

$$F_y = L\sum_{i=1}^{N_s}\int_{\theta_{sti}}^{\theta_{eti}}\left[\frac{1}{2\mu_0}\left(B_{\mathrm{l},ri}^2 - B_{\mathrm{l},\theta i}^2\right)\sin\theta + \frac{1}{\mu_0}B_{\mathrm{l},ri}B_{\mathrm{l},\theta i}\cos\theta\right]r_g d\theta \quad (32)$$

Equations (31) and (32) mean that the magnetic force of the original eccentric state is synthesized from the contribution of each concentric state. The superposition method would be more accurate but more time-consuming if the section number (N_s) of the rotor is larger. Therefore, the influence of the section number should be investigated to trade off accuracy against efficiency. This will be investigated later.

4. Results and discussions

A case study with the specifications listed in Table 1 is considered to evaluate the efficacy of the proposed analytical model for heteropolar AMB.

Table 1 HERE.

A. Calculation results without rotor eccentricity

Firstly, the air-gap magnetic flux density including radial (B_r) and tangential (B_t) components without eccentricity are obtained by the sub-domain method and compared with the results calculated by the FEM shown in Fig. 4. The comparisons of the waveforms and harmonics show that the analytical method agrees well with the FEM method when there is no rotor eccentricity.

Fig. 4(a) and Fig. 4(b) HERE.

B. Analysis of the section number of superposition method

The influence of the section number (N_s) on accuracy and efficiency for the superposition method is investigated.

Fig. 5(a) shows the waveforms of the radial components of the air-gap flux density obtained by FEM and the superposition method with different section numbers for an eccentricity factor of 0.5. The waveforms with smaller section numbers are obviously stepped, and the smoothness of the waveforms is improved as the section number increases. Fig. 5(b) further shows the calculation time and mean squared error (MSE) of the flux density in the air-gap compared to the FEM results with different section numbers for the eccentricity factor of 0.5. As the section number increases, calculation time increases and the error decreases. However, the accuracy remains unchanged when the section number more than 60. Therefore, a proper section number, i.e., 60 in this paper, can be selected accordingly to achieve fast results with decent accuracy.

Fig. 5(a) and Fig. 5(b) HERE.

C. Comparison of results from two analytical methods and FEM

Fig. 6 to Fig. 8 depict the magnetic flux density distributions in the air-gap with the rotor eccentricity factor of 0.25, 0.5 and 0.75 along the *x*-axis from the original point, respectively. The magnetic force along the *x*-axis under different eccentricity distances along the *x*-axis is evaluated by two different analytical methods as well as the FEM method with linear and nonlinear materials, and the results are compared in Fig. 9 (a). Fig. 9 (b) shows the errors of the results of two analytical methods compared to nonlinear FEM results. As is explained from these figures, the results calculated by two

different analytical methods both agree with the numerical method when the eccentricity is small. The magnetic flux density increases where the air-gap length is reduced due to the reduction of the reluctance. However, the accuracy of the perturbation method decreases with the increase of the eccentricity. It is because the perturbation method only considers up to the first-order term by omitting the high-order terms which would play a more important role when the eccentricity gets too large. As the eccentricity continues to increase, the results of the superposition method deviate from those of the nonlinear FEM while staying consistent with those of the linear FEM. It is because saturation appears in the iron core when the air-gap is too small, with which the analytical method cannot inherently deal. Considering the maximum error of 20% compared to the nonlinear FEM method, the perturbation method is valid only within the range of 0 to 0.4 eccentricity factor, while the error of the superposition method can remain under 20% even when the eccentricity factor is 0.75. Furthermore, the eccentricity factor of the practical AMB rotor is generally under 0.5 due to the limit of backup bearings; as a result, the larger eccentricity is not considered here.

Fig. 6(a) and Fig.6(b) HERE.

Fig. 7(a) and Fig. 7(b) HERE.

Fig. 8 (a) and Fig. 8(b)HERE.

Fig. 9(a) and Fig. 9(b) HERE.

D. CPU Time

In terms of the computation time, the 2D nonlinear FEM requires almost 32 seconds to obtain the magnetic flux density and magnetic force without eccentricity when the model has 23504 elements (i7-4800 MQ @ 2.70(GHz) CPU, 32 (GB) RAM). If various eccentricity conditions are considered, it will cost more time to obtain the results. In

addition, the preprocessing of FEM cost more resources and time. The perturbation method requires only 2 seconds to get the final results and the superposition method requires 7 seconds with a section number of 60. Therefore, the analytical models are much faster than FEM.

5. Conclusion

In this paper, we have presented two different analytical methods to consider the rotor eccentricity of AMB. These two AMs are widely used in AMB applications, but the pros and cons are not investigated in the previous study. The results show that the superposition method can deal with a larger eccentricity range than the perturbation method, while the latter consumes less time. In other words, this paper presented a guideline for AMB designers to analyze the eccentricity condition.

The presented work is not limited to the AMB; the study of section number of the superposition method also has an instructiveness for machine designers to analyze other types of electric machines, and it gives a clue of the trade-off between accuracy and time.

Acknowledgment

This work is supported in part by the National Nature Science Foundation of China (Project Number 51777034), “the Excellence Project Funds of Southeast University”, and State Key Laboratory of Reliability and Intelligence of Electrical Equipment (Project Number EERIKF2018009), Hebei University of Technology.

References

[1] G. Schweitzer *et al.*, *Magnetic Bearings: Theory, Design, and Application to Rotating Machinery*, Softcover reprint of hardcover 1st ed. 2009. Dordrecht ; New York: Springer, 2010.

[2] A. Rahideh and T. Korakianitis, "Analytical Open-Circuit Magnetic Field Distribution of Slotless Brushless Permanent-Magnet Machines With Rotor Eccentricity," *IEEE Trans. Magn.*, vol. 47, no. 12, pp. 4791–4808, Dec. 2011.

[3] J. Fu and C. Zhu, "Subdomain Model for Predicting Magnetic Field in Slotted Surface Mounted Permanent-Magnet Machines With Rotor Eccentricity," *IEEE Trans. Magn.*, vol. 48, no. 5, pp. 1906–1917, May 2012.

[4] F. Shakibapour, A. Rahideh, and M. Mardaneh, "2D analytical model for heteropolar active magnetic bearings considering eccentricity," *IET Electr. Power Appl.*, vol. 12, no. 5, pp. 614–626, 2018.

[5] Y. Li, Q. Lu, Z. Q. Zhu, D. Wu, and G. Li, "Superposition Method for Cogging Torque Prediction in Permanent Magnet Machines With Rotor Eccentricity," *IEEE Trans. Magn.*, vol. 52, no. 6, pp. 1–10, Jun. 2016.

[6] Y. X. Li and Z. Q. Zhu, "Cogging Torque and Unbalanced Magnetic Force Prediction in PM Machines With Axial-Varying Eccentricity by Superposition Method," *IEEE Trans. Magn.*, vol. 53, no. 11, pp. 1–4, Nov. 2017.

[7] K. Boughrara, T. Lubin, and R. Ibtiouen, "General Subdomain Model for Predicting Magnetic Field in Internal and External Rotor Multiphase Flux-Switching Machines Topologies," *IEEE Trans. Magn.*, vol. 49, no. 10, pp. 5310–5325, Oct. 2013.

[8] L. J. Wu, Z. Q. Zhu, D. Staton, M. Popescu, and D. Hawkins, "Subdomain Model for Predicting Armature Reaction Field of Surface-Mounted Permanent-Magnet

Machines Accounting for Tooth-Tips," *IEEE Trans. Magn.*, vol. 47, no. 4, pp. 812–822, Apr. 2011.

Fig. 1 Illustrative representation of a heteropolar AMB.

Fig. 2 Coordinate frames of eccentricity of the heteropolar AMB

Fig. 3 Schematic diagram of the superposition method

Fig. 4 Magnetic flux density in the air-gap without rotor eccentricity obtained by the analytical method and the FEM method. (a) waveforms (b) harmonics

Fig. 5 Influence of section number of superposition method (a) Waveforms of radial components of the air-gap flux density for 0.5 eccentricity factor (b) Calculation time and MSE of flux density in the air-gap for 0.5 eccentricity factor

Fig. 6 Result comparision with eccentricity factor 0.25 along the x-axis. (a) Magnetic flux density in the air-gap. (b) Magnetic traction force waveform versus different rotor positions.

Fig. 7 Result comparision with eccentricity factor 0.5 along the x-axis. (a) Magnetic flux density in the air-gap. (b) Magnetic traction force waveform versus different rotor positions..

Fig. 8 Result comparision with eccentricity factor 0.75 along the x-axis. (a) Magnetic flux density in the air-gap. (b) Magnetic traction force waveform versus different rotor positions..

Fig. 9 Magnetic force along the x-axis with the different eccentricity factors on x-axis (a) calculation results of two analytical methods, linear FEM and nonlinear FEM (b) errors of the results of two analytical methods compared to nonlinear FEM results.

Table 1 Specifications of a heteropolar AMB.

Symbol	QUANTITY	Values	Units
R_{sl}	the radius of the slot bottom	0.0379	m
R_s	the radius of the slot teeth	0.0159	m
R_r	the radius of the rotor yoke	0.0157	m
δ	slot span angle	0.2833	rad
L	the axial length of the AMB	0.0314	m
Q	number of slots	8	-
N	number of harmonics in the air-gap	500	-
V	number of harmonics in the slots	50	-
I	the current of each winding	2	A

Fig. 1

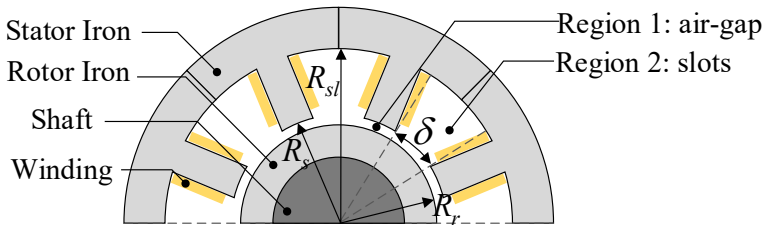

Fig. 2

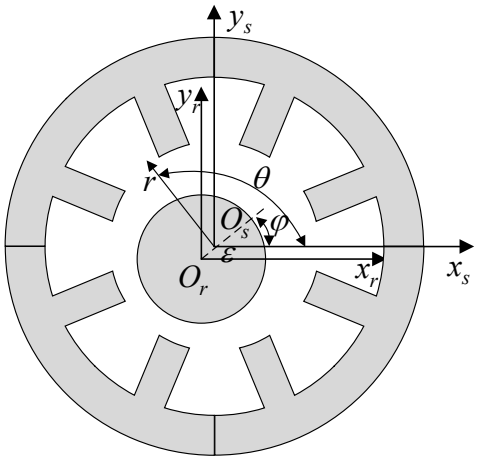

Fig. 3

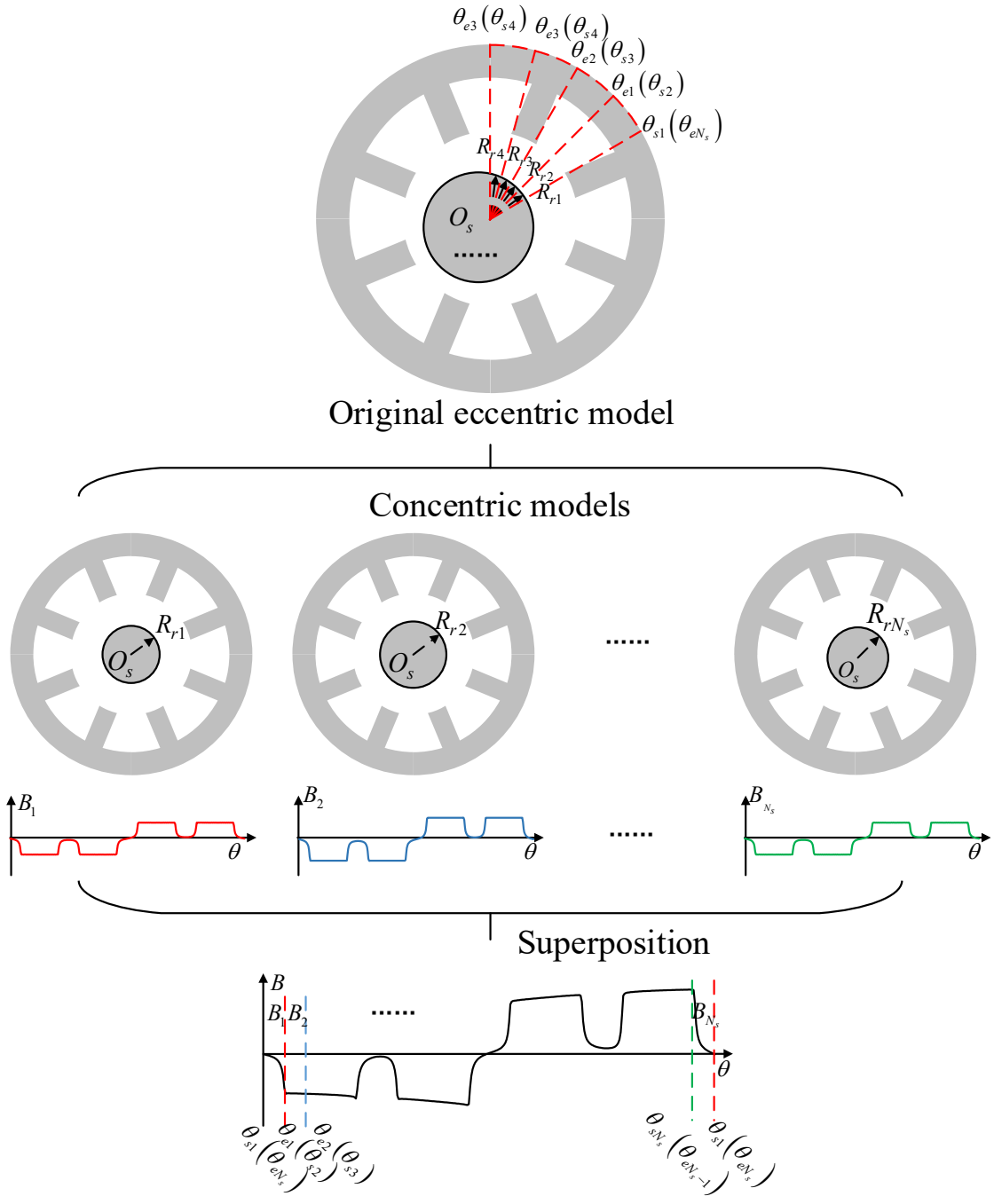
Original eccentric model
Concentric models
Superposition

Fig. 4(a)

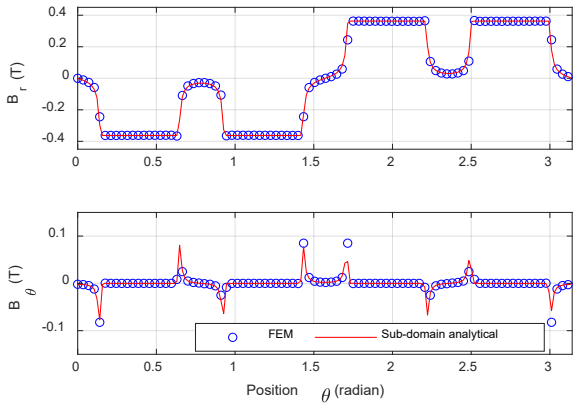

Fig. 4(b)

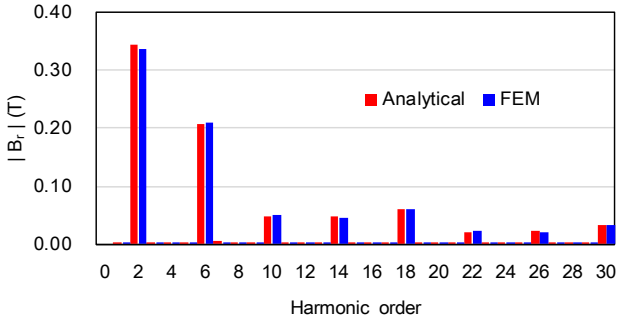

Fig. 5(a)

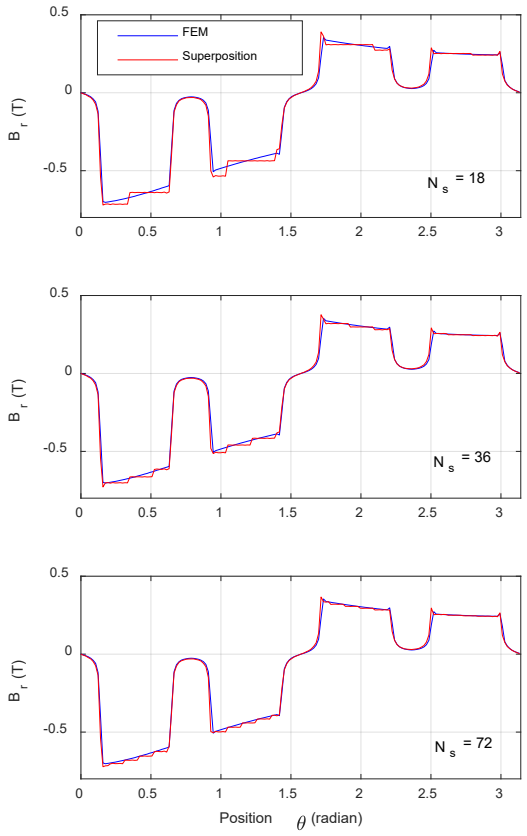
FEM
Superposition
B r (T)
N s = 18
N s = 36
N s = 72
Position θ (radian)

Fig. 5(b)

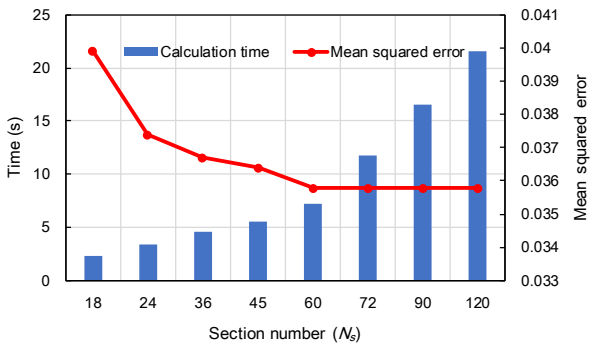
Calculation time
Mean squared error
Time (s)
Mean squared error
Section number (Ns)

Fig. 6 (a)

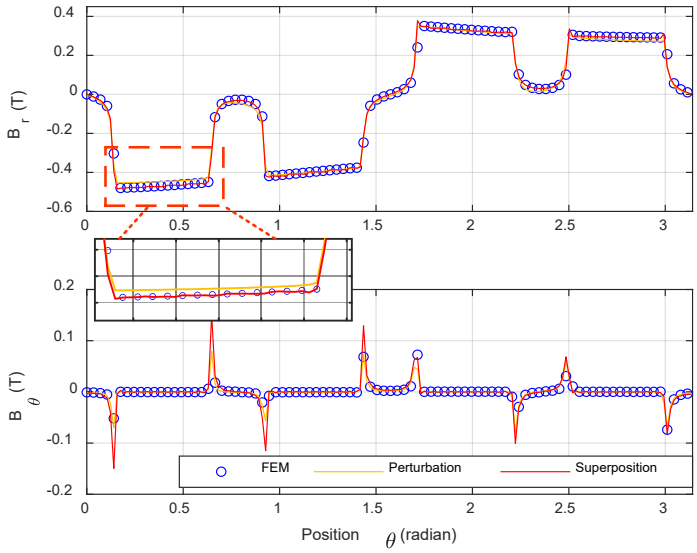
B r (T)
B θ (T)
FEM
Perturbation
Superposition
Position θ (radian)

Fig. 6 (b)

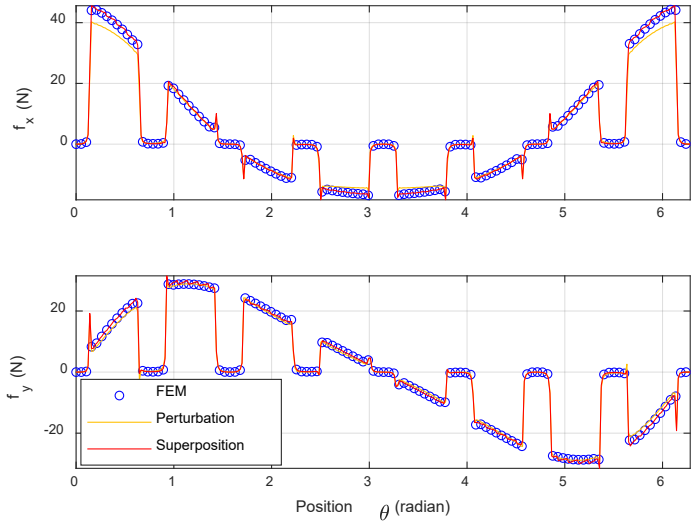
f x (N)
f y (N)
FEM
Perturbation
Superposition
Position θ (radian)

Fig. 7 (a)

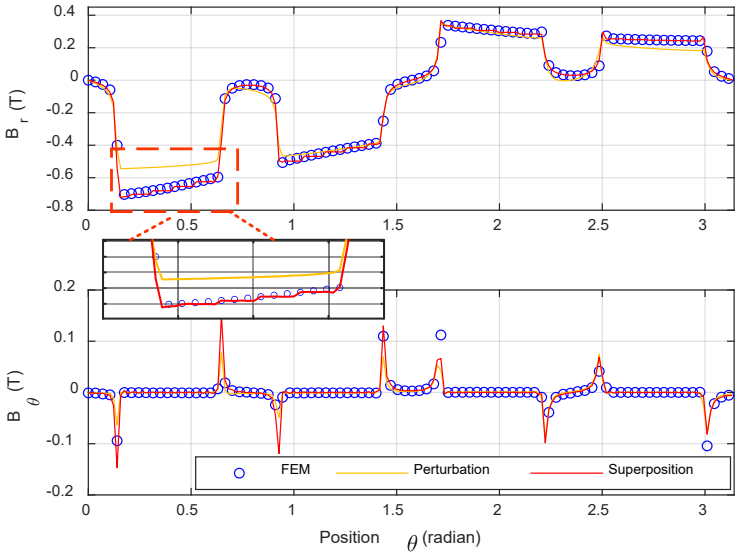
B r (T)
B θ (T)
FEM
Perturbation
Superposition
Position θ (radian)

Fig. 7 (b)

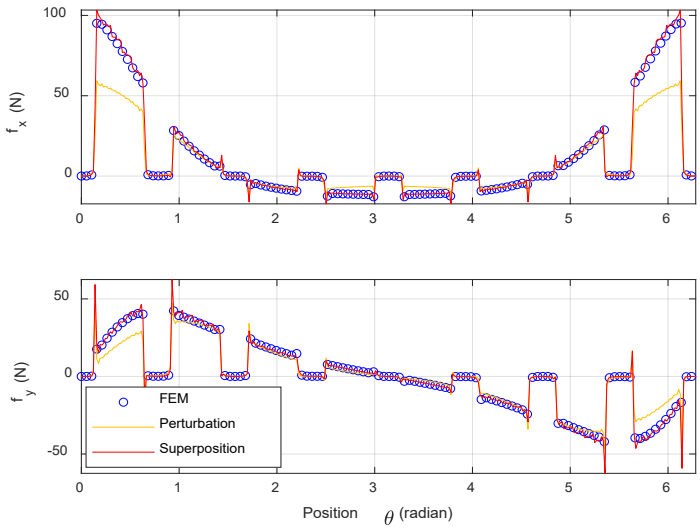
f x (N)
f y (N)
FEM
Perturbation
Superposition
Position θ (radian)

Fig. 8 (a)

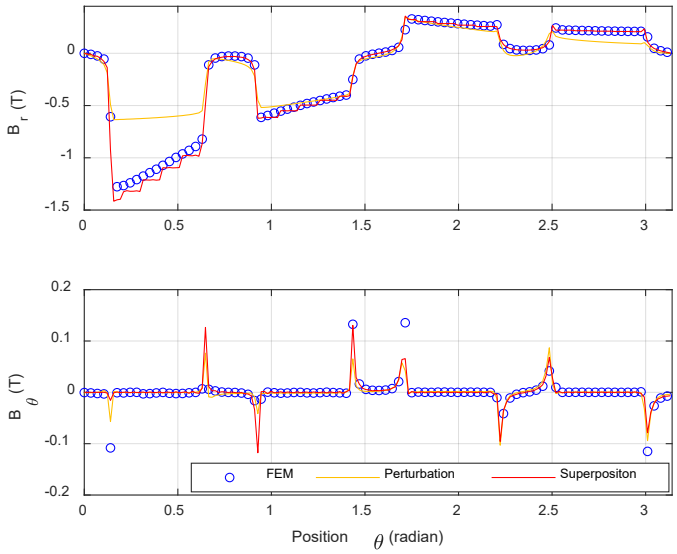
B r (T)
B θ (T)
FEM
Perturbation
Superpositon
Position θ (radian)

Fig. 8 (b)

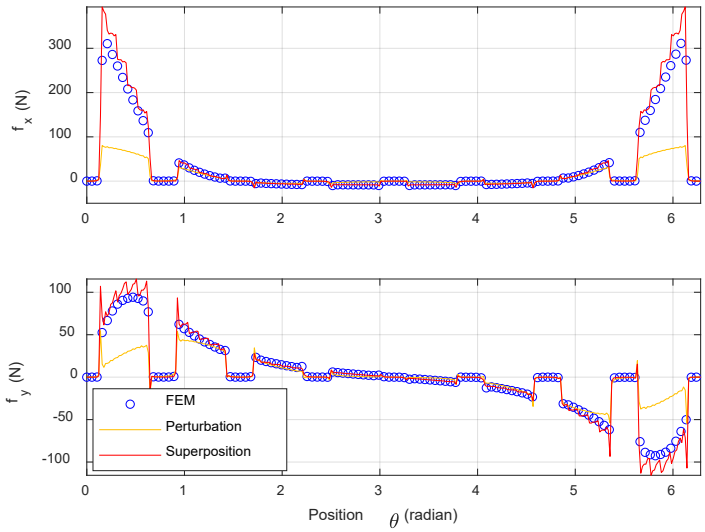
f x (N)
f y (N)
FEM
Perturbation
Superposition
Position θ (radian)

Fig. 9(a)

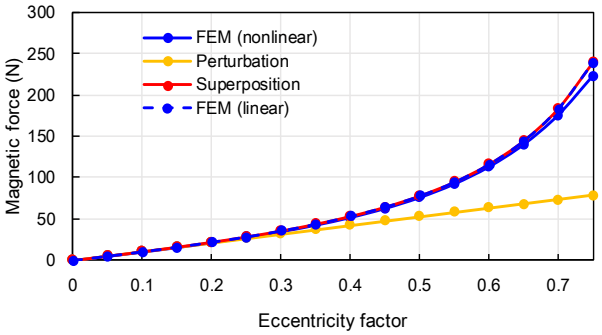
FEM (nonlinear)
Perturbation
Superposition
FEM (linear)
Magnetic force (N)
300
250
200
150
100
50
0
0
0.1
0.2
0.3
0.4
0.5
0.6
0.7
Eccentricity factor

Fig. 9(b)

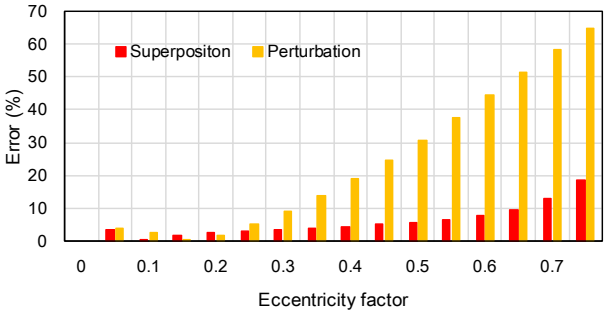
Superpositon
Perturbation
Error (%)
70
60
50
40
30
20
10
0
0
0.1
0.2
0.3
0.4
0.5
0.6
0.7
Eccentricity factor